JGR Space Physics

TECHNICAL REPORTS: DATA
10.1029/2021JA029334

Intercalibration of the Plasma Density Measurements in Earth's Topside Ionosphere

Artem Smirnov[1,2], Yuri Shprits[1,2,3], Irina Zhelavskaya[1], Hermann Lühr[1], Chao Xiong[1,4], Andreas Goss[5], Fabricio S. Prol[6], Michael Schmidt[5], Mainul Hoque[6], Nicholas Pedatella[7,8], and Mátyás Szabó-Roberts[1,2]

[1]Space Physics and Space Weather (Section 2.7), Helmholtz Centre Potsdam - GFZ German Research Centre for Geosciences, Potsdam, Germany, [2]Institute of Physics and Astronomy, University of Potsdam, Potsdam, Germany, [3]Department of Earth, Planetary and Space Sciences, University of California Los Angeles, Los Angeles, CA, USA, [4]Department of Space Physics, College of Electronic Information, Wuhan University, Wuhan, China, [5]Deutsches Geodätisches Forschungsinstitut, Technical University of Munich, Munich, Germany, [6]Institute for Solar-Terrestrial Physics, German Aerospace Center, Neustrelitz, Germany, [7]High Altitude Observatory, National Center for Atmospheric Research, Boulder, CO, USA, [8]COSMIC Program Office, University Center for Atmospheric Research, Boulder, CO, USA

Key Points:

- A systematic comparison of the plasma density data from CHAMP, C/NOFS, GRACE, COSMIC, and Swarm missions is performed
- Electron densities retrieved from COSMIC-RO agree well with GRACE-KBR observations showing a relative difference of less than 2%
- Intercalibration factors, allowing to eliminate the systematic offsets between the considered data sets, are presented

Supporting Information:

Supporting Information may be found in the online version of this article.

Correspondence to:

A. Smirnov,
artem.smirnov@gfz-potsdam.de

Citation:

Smirnov, A., Shprits, Y., Zhelavskaya, I., Lühr, H., Xiong, C., Goss, A., et al. (2021). Intercalibration of the plasma density measurements in Earth's topside ionosphere. *Journal of Geophysical Research: Space Physics*, *126*, e2021JA029334. https://doi.org/10.1029/2021JA029334

Received 10 MAR 2021
Accepted 3 SEP 2021

Abstract Over the last 20 years, a large number of instruments have provided plasma density measurements in Earth's topside ionosphere. To utilize all of the collected observations for empirical modeling, it is necessary to ensure that they do not exhibit systematic differences and are adjusted to the same reference frame. In this study, we compare satellite plasma density observations from Gravity Recovery and Climate Experiment (GRACE), Constellation Observing System for Meteorology, Ionosphere, and Climate (COSMIC), CHAllenging Minisatellite Payload (CHAMP), Swarm, and Communications/Navigation Outage Forecasting System (C/NOFS) missions. Electron densities retrieved from GRACE K-Band Ranging (KBR) system, previously shown to be in excellent agreement with incoherent scatter radar (ISR) measurements, are used as a reference. We find that COSMIC radio occultation (RO) densities are highly consistent with GRACE-KBR observations showing a mean relative difference of <2%, and therefore no calibration factors between them are necessary. We utilize the outstanding three-dimensional coverage of the topside ionosphere by the COSMIC mission to perform conjunction analysis with in situ density observations from CHAMP, C/NOFS, and Swarm missions. CHAMP measurements are lower than COSMIC by ~11%. Swarm densities are generally lower at daytime and higher at nighttime compared to COSMIC. C/NOFS ion densities agree well with COSMIC, with a relative bias of ~7%. The resulting cross-calibration factors, derived from the probability distribution functions, help to eliminate the systematic leveling differences between the data sets, and allow using these data jointly in a large number of ionospheric applications.

1. Introduction

The ionosphere is an ionized part of the upper atmosphere, spanning from 60 to around 1,000 km in altitude (Hargreaves, 1992). It arises mainly due to the photoionization effects from the solar extreme ultraviolet (EUV) radiation and charged energetic-particle precipitation (Kivelson & Russell, 1995). Generally, the ionosphere is strongly coupled with the thermosphere (Astafyeva, 2019). The latter supplies the neutral particles that can be ionized, and plays a crucial role in the interplay between the production (source) and recombination (loss) processes. The ionosphere affects the propagation of the Global Navigation Satellite System (GNSS) signals by introducing frequency-dependent delays. Unlike the neutral atmosphere, which can cause errors in navigation and positioning in the order of several meters, ionospheric effects can yield uncertainties of up to ~100 m (e.g., Hernández-Pajares et al., 2011; Petit & Luzum, 2010). Ionospheric delays are inversely related to the square of carrier frequency, and directly proportional to electron density integrated along the ray path (e.g., Goss et al., 2019; Hobiger & Jakowski, 2017).

Electron density distribution in the ionosphere strongly depends on altitude and can be divided into several layers, originally identified from ionograms: the D-layer (60–90 km altitude), E-layer (90–130 km), and F-layer (above 130 km), which can be subdivided into F1 and F2 layers (e.g., Astafyeva, 2019). The dominant contribution to electron density profiles comes from the peak of the F2 layer, generally located between

~250 and 400 km in altitude. The part of the ionosphere located above the F2-peak altitude is referred to as the topside ionosphere; it has a smooth transition into the plasmasphere at approximately 800–1,000 km in altitude. Previous studies have indicated that the topside ionosphere and the plasmasphere are a major constituent of the vertical total electron content (vTEC), accounting for up to >60% of the vTEC magnitude (e.g., Cherniak et al., 2012; Klimenko et al., 2015; Lee et al., 2013; Yizengaw et al., 2008). The F2-peak density (NmF2) and the peak height (hmF2), due to their importance for radio operation, have received a lot of attention in terms of data quality. The existing empirical models, including the International Reference Ionosphere (IRI) (e.g., Bilitza, 2018; Bilitza & Xiong, 2021) and NeQuick (e.g., Nava et al., 2008), give an accurate representation of these parameters. In the topside ionosphere however, the altitude coverage of observations is highly non-uniform. This results in the notable discrepancies between observations and model predictions above hmF2 (e.g., Cherniak & Zakharenkova, 2019; Kashcheyev & Nava, 2019). To develop high-resolution empirical models of electron density, it is crucial to have dense coverage of inter-calibrated observations in the topside ionosphere.

Ionospheric density profiles have been traditionally monitored through a network of ground-based ionosondes which provide electron density values from ~60 km up to the height of the F2 density peak. Observations of the topside densities were at first provided by the incoherent scatter radars (ISRs) and vertical topside sounders on board several missions (e.g., Alouette) in the 1960–1970s (Benson & Bilitza, 2009). These observations were, however, very sparse, both temporally and spatially (e.g., Prol et al., 2019). The traditional ground-based observational techniques have been providing accurate and reliable measurements of ionospheric density and temperature for several decades. Yet, the ionosondes and especially ISRs are only available at a limited number of sites around the globe, and therefore these instruments alone cannot satisfy the increasing demand for high-resolution electron density data, even more so in the topside ionosphere. Over the last 50 years, in situ satellite observations at low Earth orbit, mainly by Langmuir probes (LPs) and retarding potential analyzers (RPAs), have become an important data source. However, these observations are bound to the orbit of their specific spacecraft, and therefore also cannot provide the global three-dimensional coverage of the ionosphere. The GNSS radio occultation (RO) represents the only active observational technique to date that allows profiling through the entire F-layer of the ionosphere with global coverage (e.g., Cherniak & Zakharenkova, 2014). It has been estimated that the precision of the RO observations is $\sim 10^3 \mathrm{cm}^{-3}$ (Schreiner et al., 2007), although the RO profile geometry and assumptions introduced during the density retrieval can lead to an underestimation of the Equatorial Ionisation Anomaly (EIA) crests on the order of $\sim 10^4 - 10^5 \mathrm{cm}^{-3}$ (e.g., Liu et al., 2010; Yue et al., 2010).

A large number of studies have analyzed the agreement between various plasma density data sets in the Earth's ionosphere. In particular, the RO data from the Constellation Observing System for Meteorology, Ionosphere, and Climate (COSMIC) mission, comprising a fleet of six satellites, have been validated extensively by ground-based observations. Lei et al. (2007) compared preliminary COSMIC observations of electron density to the ISR data and reported that the two were largely consistent in the topside, although the number of points for the comparison was limited. COSMIC NmF2 observations were found to correspond well with Arecibo ISR measurements (Kelley et al., 2009). Similar conclusions were obtained by Cherniak and Zakharenkova (2014) for Kharkov ISR. Chuo et al. (2011) compared the F2-peak parameter observations by the Jicamarca digisonde with those by COSMIC-RO based on data from 2006 to 2008. RO and digisonde NmF2 observations were found to agree well, with a correlation of 94% and near-zero bias. Habarulema and Carelse (2016) performed a comparison of NmF2 and hmF2 between COSMIC and ionosonde data specifically during the geomagnetic-storm times (with Dst< −50 nT). It was found that the precision of COSMIC-RO data did not degrade during geomagnetically active times, compared to the quiet times. Furthermore, several studies performed comparisons of the electron density profiles (EDPs) from RO-devoted missions. For instance, Forsythe et al. (2020) used RO data retrieved from the Spire constellation, comprising 84 satellites, to compare with COSMIC EDPs and reported a close agreement between them. The RO observations by the China Seismo-Electromagnetic Satellite (CSES) were recently found to also be in very good agreement with COSMIC (Wang et al., 2019).

Several studies have performed comparisons between the in situ satellite and ground-based observations. McNamara et al. (2007) compared plasma frequency observations from the CHAllenging Minisatellite Payload (CHAMP) mission and Jicamarca ionosonde. Although generally, the two data sets were in good

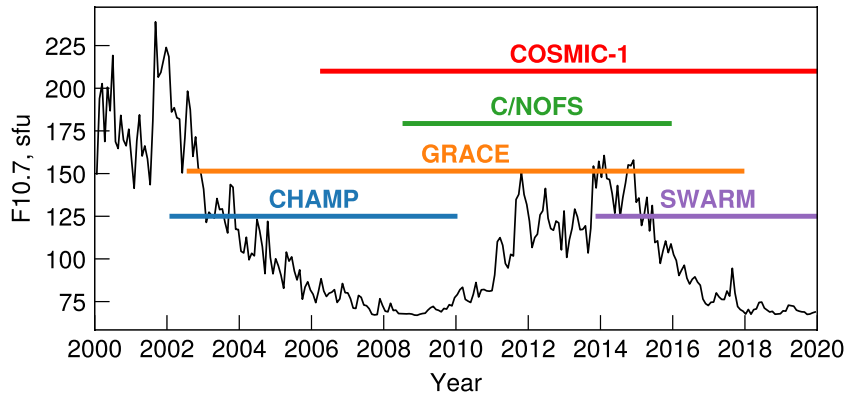

Figure 1. Temporal coverage of the missions used in this study.

agreement, CHAMP LP densities were on average lower by ~4.6%. Recently, Lomidze et al. (2018) compared Swarm Langmuir probe observations to Jicamarca, Arecibo and Millstone Hill ISRs, based on the overhead passes from December 2013 to June 2016. Plasma frequencies measured by Swarm-LP were lower by ~10%, which corresponds to a 21% underestimation of electron density. The study showed that the application of ISR-derived corrections to Swarm Langmuir probe data improved the agreement with the COSMIC RO measurements. A number of other studies have presented comparisons between RO and Langmuir probe data. Pedatella et al. (2015) compared COSMIC RO densities with in situ measurements by Communications/Navigation Outage Forecasting System (C/NOFS) and CHAMP, however, no inter-calibration factors were introduced in that study. Lai et al. (2013) analyzed conjunctions between C/NOFS and COSMIC data and reported a close agreement between the two, although the study was based on a small number of conjunctions occurring on 2 consecutive days.

The aim of the present study is to compare electron density data from several missions collected over the past 20 years and adjust them to the same reference frame. This is a necessary step to aid future empirical modeling and data assimilation efforts. Most of the studies mentioned above utilized only a single pair of instruments or observational techniques for comparisons, while in this study, we use data from five satellite missions that operate on different observational principles. The ground-based ISR observations, which comprise the golden standard plasma density data set in the topside ionosphere, cannot provide enough spatial and altitude coverage to perform the intercalibration. In this study, we use electron densities retrieved from the Gravity Recovery And Climate Experiment (GRACE) K-Band Ranging (KBR) system as a reference. The KBR densities have been calibrated by ISRs at Arecibo, Millstone Hill, Jicamarca, and EISCAT and shown to be in excellent agreement with ISR observations (Xiong et al., 2015). Furthermore, due to their retrieval procedure, KBR densities do not experience quality degradation throughout the mission's lifespan. We compare the COSMIC RO electron densities to the GRACE-KBR data at a large number of conjunctions (> 7100) and find that the two data sets are in very good agreement with a mean relative difference of ~1.6%. Missions providing in situ density observations (e.g., CHAMP, C/NOFS, and Swarm) operate at different altitudes, and require a three-dimensional data set to be calibrated against. After establishing that COSMIC concurs with GRACE-KBR, the in situ measurements of plasma density by the CHAMP, C/NOFS, and Swarm missions are compared to COSMIC and the cross-calibration factors between them are introduced. The study consists of five parts, including this introductory section. In Section 2, we describe the data used in this study. Section 3 is concerned with the methodology. Results are presented in Section 4. The final section draws conclusions and discusses potential applications of the intercalibrated observations.

2. Data Set

In this section, we describe the data sources used in the present study. The temporal coverage of the missions with respect to solar cycles 23 and 24 is shown in Figure 1, and their altitude range of measurements and horizontal spatial resolutions are specified in Table 1. We first describe the GRACE-KBR electron densities,

Table 1
Horizontal Spatial Resolution and Altitude Range of Measurements Used in This Study

Mission	Altitude range	Horiz. spatial resolution, km
GRACE/KBR	400–550	~200
COSMIC/RO	150–800	~300
CHAMP/PLP	300–460	~115
CNOFS/CINDI	400–850	3.8
Swarm A/LP	460–490	3.8
Swarm B/LP	490–510	3.8
Swarm C/LP	460–490	3.8

Note. CHAMP, CHAllenging Minisatellite payload; CINDI, Coupled Ion Neutral Dynamics Investigation; COSMIC, Constellation Observing System for Meteorology, Ionosphere, and Climate; GRACE, Gravity Recovery and Climate Experiment; KBR, K-Band Ranging; LP, Langmuir probe; PLP, Planar Langmuir Probe; RO, radio occultation.

used as a reference for the intercalibration. Then, the RO electron densities from the COSMIC constellation, and in situ observations by CHAMP, Swarm, and C/NOFS are described.

2.1. GRACE-KBR Electron Densities

The GRACE mission was launched in March 2002 into a near-circular polar orbit with an inclination of 89° and initial altitude of ~490 km. The mission consisted of two identical spacecraft, GRACE-A and GRACE-B, following each other at a distance of ~200 km. The local time of the mission precessed by 4.5 min per day, thus providing coverage of all local times every 160.5 days (e.g., Xiong et al., 2010). While the primary purpose of the GRACE mission was to construct global high-resolution and time-dependent models of the Earth's gravity field, the satellites were equipped with the KBR system which also allowed the derivation of electron density. The brief description of the electron density reconstruction is given below and the full explanation is provided in Xiong et al. (2010, 2015).

The KBR is one of the core instruments of the GRACE mission; it measures the dual one-way range changes between the two satellites with a precision of 1μm. The level 1B KBR data include an ionospheric correction which can be used for deriving the horizontal total electron content between the two satellites. Furthermore, the position of the two GRACE spacecraft is provided in the GPS Navigation (GNV) data. By dividing the horizontal TEC by distance, the average electron density between the two spacecraft can be retrieved with a resolution of approximately 170–220 km along the ground track (Xiong et al., 2010). However, it is of note that there is an unknown bias in the ionospheric correction term, which also remains in the derived electron density, but this bias is constant for continuous intervals of GRACE measurements and can be eliminated by using the reference data set. Xiong et al. (2015) used several ISRs, namely EISCAT at Tromsø and Svalbard locations, Arecibo, and Millstone Hill to validate the GRACE density measurements. The retrieved KBR electron densities were in excellent agreement with ISR observations, having a correlation of more than 97% and a very low bias of $3 \cdot 10^4$ el./cm^3.

ISRs are one of the oldest traditional instruments for studying the topside ionosphere and have been in use for decades. Due to the near-zero bias of GRACE-KBR density data with respect to the ISR observations, GRACE electron densities comprise a practically calibration-free data set at altitudes 400–500 km, covering ~1.5 solar cycles (2002–2017). Therefore, in the present study GRACE-KBR measurements are used as a reference for intercalibration with other data sources. Using the ISR data alone would not provide enough spatial coverage for the intercalibration, as only a very limited number of the overhead passes can be found for each of the missions. We use GRACE-KBR observations from 2006 to 2015 to compare with COSMIC RO data.

2.2. COSMIC Radio Occultation Measurements

The GNSS RO measurements represent a remote sensing technique allowing retrieval of high-resolution vertical profiles of the atmosphere and ionosphere (e.g., Melbourne et al., 1994; Schreiner et al., 2007). By means of the GPS/MET satellite, it was experimentally shown that RO can be used for deriving the vertical electron density profiles (Hajj et al., 1996). In context with the CHAMP satellite launched a few years later, the RO analysis technique was fully developed for both ionospheric and atmospheric profiling, and the first software package for routine operational evaluation of GPS/RO data was created (Jakowski et al., 2002). Since then, electron density profiles retrieved from ROs have become a major source of observations used in various ionospheric applications (Pedatella et al., 2015). The RO missions provide ionospheric profiles from the D-layer up to satellite height and thus give a representation of the three-dimensional structure of the ionosphere. Electron density profiles are retrieved using the Abel inversion with several underlying assumptions, including the proportionality between refractivity and electron density, straight-line signal

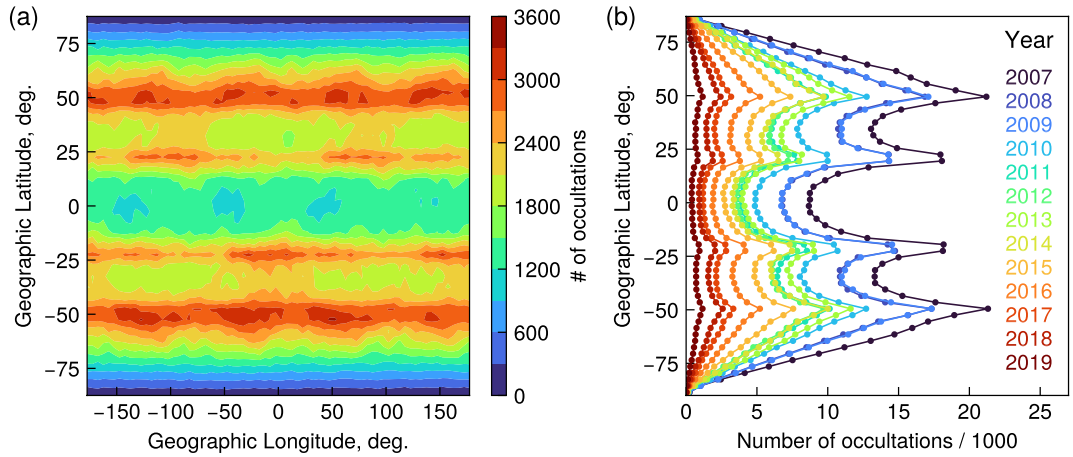

Figure 2. (a) Global distribution of the number of occultations observed by the COSMIC-1 mission per 5° × 5° bins in terms of geographic latitude (GLat) and longitude (GLon) for the mission's entire lifespan, with a contour function applied to the plot. (b) Number of COSMIC-1 radio occultations as a function of latitude in 2007–2019.

propagation, and spherical symmetry (e.g., Schreiner et al., 2007). Although the latter assumption can cause systematic errors in the retrieved densities (e.g., Yue et al., 2010), RO electron densities have been thoroughly validated by ground-based instruments (e.g., Cherniak & Zakharenkova, 2014; Lei et al., 2007; Schreiner et al., 2007).

Multiple spacecraft have supplied the EDP data by means of the RO technique. The largest data source up to date, both in terms of the number of occultations and temporal coverage, is provided by the COSMIC mission. RO-devoted constellations that preceded COSMIC provided much fewer data points, and were estimated to comprise only up to several percent of the COSMIC data set. The COSMIC mission consisted of six microsatellites in 72° inclination orbits. The satellites were launched at the beginning of 2006 with an initial altitude of approximately 500 km, which was increased up to 800 km throughout the following 1.5 years. This created a spatial separation of ∼30 degrees between the orbital planes (Lei et al., 2007). Each of the COSMIC satellites carried on board the GPS occultation experiment (GOX) receiver that enables probing the Earth's atmosphere using the RO technique.

One of the notable features of the COSMIC mission is the open-loop mode of tracking both the rising and setting occultations, which approximately doubles the number of profiles and thus provides a denser coverage of the ionosphere (Schreiner et al., 2007). At the beginning of the mission's lifespan, the COSMIC constellation was providing >2,500 EDPs per day, while the number gradually reduced to 200–300 profiles by the end of the mission in 2019 (e.g., Wang et al., 2019). The total number of the COSMIC profiles used in this study exceeds 4.5 million. It is of note that most of the COSMIC occultation events occurred at mid-latitudes, while the equatorial region generally has fewer data points (Figure 2, see also Arras et al., 2010). The follow-up mission COSMIC-2 has been launched in 2019 and mainly focuses on probing the lower equatorial latitudes, providing ∼5,000 ROs per day. The preliminary data quality analysis (Cherniak et al., 2021; Schreiner et al., 2020) has already demonstrated promising results for ionospheric monitoring, and using these data for the intercalibration can be a topic for further studies.

As described in Section 1, the traditional ground-based observational techniques suffer from limited data coverage, both in terms of their location on the globe and in altitude. The electron density profiles retrieved from ROs are deprived of these limitations and provide a global three-dimensional data set of electron densities. Furthermore, in order to set up empirical models based on the large-scale statistics, it is essential to include the RO measurements for the topside ionosphere, where they would constitute the main and largest data source. In our study, we first compare COSMIC electron densities with the selected reference data set (GRACE-KBR). In Section 4 it is shown that the two data sets agree very well, and therefore other data sources are compared to COSMIC-1.

The COSMIC RO data were obtained from University Corporation for Atmospheric Research (UCAR) through the COSMIC Data Analysis and Archival Center (CDAAC). In this study, we use the level 2 EDPs, provided through the "IonPrf" product (https://cdaac-www.cosmic.ucar.edu/).

2.3. In Situ Plasma Density Measurements

In this study, we consider in situ observations by Langmuir probes and retarding potential analyzers. In general, a Langmuir probe is an electrode, either of planar, cylindrical, or spherical shape, which is extended into the plasma (Hargreaves, 1992). By applying a variable voltage (V) to the probe, the corresponding current (I) between the probe and the spacecraft is measured. Plasma parameters are retrieved from the current-voltage, or I-V characteristics (Knudsen et al., 2017). It should be noted that the spacecraft are subject to the sheath effect, which alters the properties of the plasma within the Debye length, and therefore the mounting posts should provide enough spatial separation between the probe and the spacecraft. The RPA is a modification of the Langmuir probe, in which one or more grids, biased at different potentials, are mounted before the collecting electrode to exclude electrons of certain energies from reaching the collectors (Hargreaves, 1992).

The CHAMP mission was launched in July 2000 into near-polar orbit with an inclination of 87.25° (e.g., Reigber et al., 2004; Rother et al., 2010). The initial orbit altitude was around ~460 km, and slowly decayed to <300 km at the end of the mission's lifespan in 2010. The orbital plane precessed by 1 h of local time in approximately 11 days, thus covering all local times in roughly 130 days when combining the ascending and descending orbital arcs (e.g., Rother et al., 2010). Among the instrumental payload aboard the CHAMP satellite, there was a Digital Ion Drift Meter (DIDM) suite, consisting of an ion drift meter (DM) and a Planar Langmuir Probe (PLP). While the DM experienced damage during the satellite ascent and also the subsequent degradation, the PLP instrument provided measurements of electron/total ion density, electron temperature, and spacecraft potential throughout the mission's entire lifespan (e.g., McNamara et al., 2007). The PLP was mounted on the lower front panel of the spacecraft pointing in the ram direction (Reigber et al., 2004). The CHAMP-PLP represented a golden rectangular plate with a 106 × 156 mm sensing area. The instrument was operating in a voltage sweep mode, taking measurements every 15 s, of which the spacecraft potential was tracked for 14 s and then the voltage was swept for another second to obtain the electron density and temperature (McNamara et al., 2007). CHAMP's orbital configuration and velocity of ~7.6 km/s correspond to the horizontal density resolution of approximately 115 km (Rother et al., 2010) (see also Table 1). The PLP design and operation are described in more detail in McNamara et al. (2007) and Rother et al. (2010).

The Swarm constellation (Friis-Christensen et al., 2006), launched on November 22, 2013, consists of three identical spacecraft following a near-polar circular orbit. During the commissioning phase, the three satellites Alpha, Bravo, and Charlie (also referred to as A, B, and C, respectively), were flying in a configuration following one another at a similar altitude of ~490 km. By April 2014, Swarm A and C satellites were lowered to 460 km, while probe B was raised up to 510 km in altitude. The primary objective of the Swarm mission is to provide highly accurate measurements of the geomagnetic field. The three satellites are also equipped with Langmuir probes to take the magnetic field perturbations arising from the diamagnetic effect into account (Friis-Christensen et al., 2006). Swarm LP represents spheres of 4 mm radius mounted on 8 cm posts at the bottom front side of the satellites. Each of the satellites is equipped with two probes—a high-gain nitrated-titanium probe used for electron density estimation, and a low-gain golden probe providing measurements of the spacecraft potential (Knudsen et al., 2017). It has been noted that the Langmuir probes configuration on Swarm is rather unconventional, both in their design and usage of the so-called "harmonic" mode, where the voltage changes harmonically at a nominal frequency of 128 Hz. In particular, the length of the LP posts is only a few centimeters, and therefore the Langmuir probes might remain within the spacecraft's Debye sheath, and therefore will not give an accurate representation of density under certain conditions. The ion density data used in this study (version "0502" of the "EFIx_LP_1B" product) are measured with the 2 Hz sampling rate, which corresponds to the spatial resolution of ~3.8 km (Table 1).

The C/NOFS satellite was launched into orbit in early 2008. The spacecraft followed an elliptical low Earth orbit (LEO), with inclination of approximately 13° (de La Beaujardière et al., 2004). The satellite altitude was between 400 and 850 km, and its orbit covered all local times. Among the scientific payload, the Coupled Ion

Neutral Dynamics Investigation (CINDI) suite, operated by NASA, contained the RPA and an ion drift meter and measured the electron temperature, drift velocities, plasma composition, and the ion number density in the topside ionosphere (Heelis et al., 2009). The satellite velocity was ~7.5 km/s (Costa et al., 2014), and the sampling rate of the CINDI/RPA instrument was 2 Hz (Coley et al., 2010), which is equivalent to the spatial resolution of around 3.8 km (Table 1).

3. Methodology

The intercalibration presented in this study is conducted in two stages. First, we select the GRACE-KBR electron density data as a reference and evaluate whether the COSMIC-RO observations agree with GRACE at a number of conjunctions along the GRACE orbit. In Section 4, we will demonstrate that the two data sets agree well, with a bias on the order of <2% and a correlation of 96%. At the second stage, it is necessary to compare other measurements against the reference. Since COSMIC is the only data set capable of providing the three-dimensional coverage of the topside ionosphere and also presents a significant interest for empirical modeling, the available in situ observations are compared with COSMIC.

To perform the above-mentioned comparisons, it is necessary to impose spatial and temporal conjunction criteria. Several studies have performed comparisons of electron density from RO and in situ observations using different coincidence criteria. Lei et al. (2007) used measurements within 6° geographic latitude (GLat) and 6° geographic longitude (GLon) for comparison of COSMIC densities with ISRs at Millstone Hill, and within $3° \times 9°$ for comparisons with Jicamarca ISR. Pedatella et al. (2015) employed observations within ±2° GLat and GLon and 15 min universal time (UT). Shim et al. (2008) estimated the meridional and zonal correlations lengths. It was found that the correlation lengths in latitude were on the order of 2° to 5°, while in longitude the values were much larger, up to 10° – 23°, based on local time and latitude (Shim et al., 2008; Wang et al., 2019). The appropriate conjunctions should be within the correlation distances (Wang et al., 2019). In the present study, we select the following conjunction criteria. We select observations coming from $\pm 1.25° \times 2.5°$ GLat and Glon and ±7.5 minutes universal time, to ensure that the observations in question are close in location and time, within distances not affected by significant horizontal ionospheric gradients. We further remove points coming from geomagnetically active times (i.e., Kp > 3) to avoid the storm-time disturbances, although it is of note that COSMIC electron density profiles have been shown to provide high-quality observations during active times as well as quiet times (Habarulema & Carelse, 2016). The unified conjunction criteria are used for all of the comparisons.

Each of the selected data sources provides daily files with electron density measurements, except for COSMIC which provides one file per individual occultation event (i.e., ~2,000 files per day at the beginning of the mission and ~200 files in 2019, see Figure 2b). Therefore, the data analysis procedure is as follows. The orbit height corresponding to the in situ measurements is interpolated onto the times of RO events. After that, we linearly interpolate the COSMIC density, as well as position in geographic latitude and longitude, onto the derived altitude. The geographic latitude and longitude corresponding to COSMIC events are then compared to orbital tracks of another satellite to check whether a conjunction occurs. If an event meets the conjunction criteria, it is added to the resulting data frame.

The scatter plots of electron density, shown in Figures 3 and 5–7a, give information about the approximate data distribution and individual conjunctions. However, it is also important to evaluate how the data sets are distributed with respect to each other by means of the probability distribution functions. Therefore, in Figures 3 and 5–7b, we show the normalized occurrence plots. We divide the x-axis into a number of intervals, and for each column, the resulting conjunctions are also divided into the same number of bins in y-direction. Then, the number of occurrences in each bin is counted and divided by the total number of points in the corresponding interval on the x-axis. Therefore, the probabilities along each bin in x-direction sum up to 1. We then introduce linear fits to the maxima of these normalized occurrences, which allows for the more correct trend estimation in the presence of outliers. Since for the linear regression it is assumed that any error present in the data set lies exclusively in the y-values, when using regression for calibration purposes the fits are performed in reverse (i.e., the reference data set is on the x-axis and the data being calibrated—on the y-axis; e.g., Moosavi & Ghassabian, 2018). When the linear relationship between the variables is formulated as $y = ax + b$, the final expression for the calibrated data takes the form:

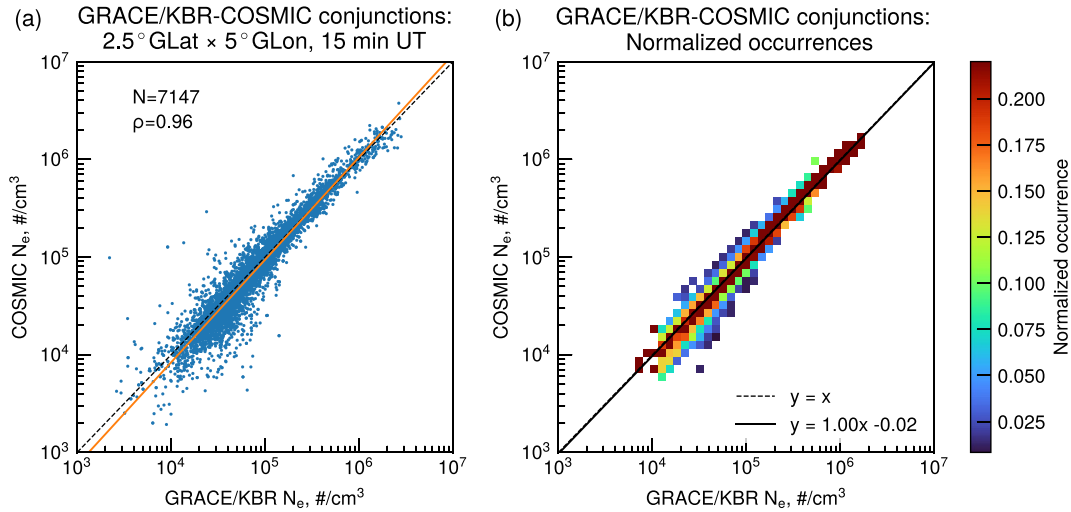

Figure 3. Comparison between COSMIC-RO and GRACE-KBR electron densities. (a) Scatter plot of GRACE-KBR versus COSMIC-RO electron densities. The black dashed line shows the one-to-one correspondence between the two data sets, and the orange-colored solid line represents the linear trend, fitted to the scatter plot. (b) Normalized occurrence plot of GRACE-KBR versus COSMIC-RO densities. In each bin in the abscissa, the maximum of the probability distribution function was selected and the linear equation was fitted to these maxima. The resulting trend is shown as a black solid line, and the equation is shown at the bottom right of the panel, with x and y representing the logarithms of GRACE and COSMIC densities, respectively. The black dashed line shows the one-to-one correspondence between two data sets.

$$y_{\text{calibrated}} = cy + d, \tag{1}$$

where $c = 1/a$ and $d = -b/a$. Table 3 gives c and d values for each of the missions allowing to calibrate the data to the reference using Equation 1.

4. Results

4.1. Comparison of GRACE-KBR and COSMIC-RO Electron Densities

Figure 3 shows a comparison between the COSMIC-RO and GRACE-KBR electron densities. Using the conjunction criteria described in Section 3, we find more than 7,100 quiet-time conjunctions between the GRACE orbital tracks and COSMIC tangential lines. From Figure 3a, it is apparent that the two data sets are in very close agreement. The dashed black line shows the one-to-one correspondence between the data sets, and the majority of points are clustered along the line. The orange-colored line gives the linear fit, performed in double-logarithmic scale. The fitted trend is generally close to the one-to-one line, although at low densities ($<3 \cdot 10^4$el./cm^3) several outliers are present, presumably due to the plasma bubbles occurring at nightside and small-scale ionospheric irregularities not resolved by COSMIC-RO. To remove those effects from the linear trend, in Figure 3b, we show the normalized occurrence histogram. In double-logarithmic scale, the data are divided into 50 bins in x- and y-directions, and bins with less than five points are removed. Then, the number of points in each bin is divided by the total number of occurrences in the corresponding interval along the x-axis. By looking at the probability in each bin of GRACE-KBR electron density, one can examine how the corresponding COSMIC-RO observations are distributed. Therefore, Figure 3b essentially represents a 2D probability distribution function of the conjunctions. Such a representation also helps to avoid overplotting when the number of conjunctions is sufficiently large. It can be seen that the largest normalized occurrence values are clustered along the one-to-one correspondence line. The linear trend equation is fitted to the normalized occurrence histogram as follows. For each interval on the x-axis (GRACE-KBR densities), we find the maximum of the probability distribution; then, the orthogonal-distance least-squares fit is performed based on the selected probability distribution maxima. The resulting trend is shown as a solid black line. It can be seen that generally, the trends based on scatter plot and

Table 2
Metrics Evaluated for the Conjunctions Between Satellites

Comparison	Mean bias, el./cm^3	Mean bias, %	Median bias, el./cm^3	Median bias, %	St. deviation, el./cm^3	Standard deviation,%	Spearman correlation,%
GRACE/KBR - COSMIC/RO	−1,813	−2	2,703	3	63,495	43	96
COSMIC/RO - CHAMP/PLP	−17,754	−10	−14,055	−12	51,151	29	96
COSMIC/RO - CNOFS/CINDI	−16,021	−6	−5,458	−7	127,468	48	97
COSMIC/RO - Swarm A/LP	−29,587	−14	−11,915	−11	82,727	45	93
COSMIC/RO - Swarm B/LP	−11,303	−8	−4,046	−5	82,762	55	86
COSMIC/RO - Swarm C/LP	−32,305	−15	−14,142	−13	92,376	43	93

2D probability distribution are quite similar, although the latter method is more stable due to the outlier removal.

The agreement between the two data sets needs to be evaluated by several metrics. For all comparisons in this study, we use the mean and median bias, both in units of density and normalized, standard deviation, and Spearman rank correlation (ρ). The values of these metrics for all comparisons are given in Table 2, and the metrics definitions are given in the Supporting Information S1. In case of COSMIC-GRACE comparison, we find that the mean value of difference between the two data sets (i.e., the mean bias) equals −1,813 el./cm^3, and a median bias of 2,704 el./cm^3. The mean and median biases normalized are 1.6% and 3%, respectively. The two data sets are in very good agreement and their relative differences are within precision of observations, which for COSMIC-RO was estimated to be in the order of 10^3 el./cm^3 (e.g., Schreiner et al., 2007). Another metric evaluated for the conjunction analysis is the correlation between the data sets. It has been demonstrated that the linear Pearson correlation can be affected by data noise, whereas the Spearman rank correlation is a more robust metric in the presence of outliers (e.g., Smirnov et al., 2020). The value of the Spearman correlation for GRACE-COSMIC comparison is high (0.96), also illustrating that the two data sets closely agree with each other.

Figure 4 demonstrates the COSMIC-RO and GRACE-KBR electron densities at conjunctions and their difference, binned by magnetic latitude (MLat) and local time (LT). To obtain a sufficiently high number of collocations in each MLat-LT interval, we bin the data by 5° Mlat and 1.5 h LT. Figure 4d shows the corresponding distribution of conjunctions. In general, conjunctions were more frequent at middle latitudes, and fewer conjunctions were observed around the geomagnetic equator. This effect comes from the spatial distribution of the COSMIC measurements, illustrated in Figure 2. The bins with less than two conjunctions were removed from the analysis, and the average number of occurrences in a bin across all magnetic latitudes and local times equals 12.

From Figures 4a and 4b, it is evident that GRACE-KBR and COSMIC-RO measurements at conjunctions are largely consistent. As noted above, the mean bias between GRACE and COSMIC measurements across all latitudes and local times is on the order of <2%. It is also important to analyze the bias distribution in the MLat-LT frame, shown in Figure 4c. It is evident that the difference between the two data sets is close to zero at middle latitudes, while in the equatorial region at ~12–18 h local time, COSMIC underestimates the crests of the equatorial ionization anomaly, and slightly overestimates the regions poleward from the crests. It should be noted, however, that the conjunction number at the equatorial latitudes is rather small, and the fountain effect is not well-resolved. The bias distribution in Figure 4c concurs with the previous study by Yue et al. (2010), which found that due to the profile geometry and assumptions introduced during the Abel inversion, the RO technique can underestimate electron densities around the EIA crests. We note, however, that in case of the GRACE-COSMIC comparison, the magnitudes of errors are relatively small, with an average value of ~$0.3–0.4 \cdot 10^5$el./cm^3, which corresponds to ~1.7 MHz when converted to the plasma frequency. Furthermore, EIA is the region where the largest density values (>$4 \cdot 10^5$el./cm^3) in the F2 layer are manifested, and the mean bias around the EIA crests in Figure 4c remains on the order of less than 10%. Therefore, although the Abel inversion introduces a slight underestimation of the EIA crests in COSMIC data, in general, the difference between COSMIC and GRACE is very small and is close to zero.

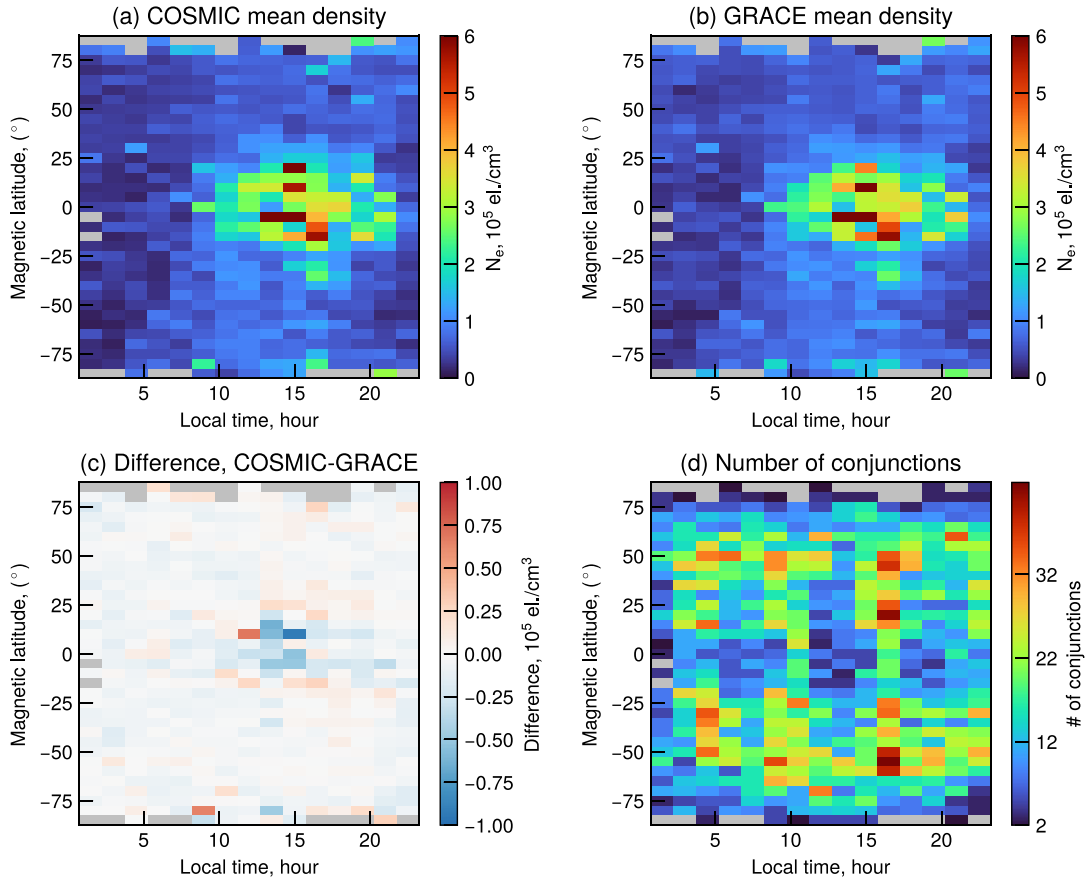

Figure 4. Comparison of COSMIC-RO and GRACE-KBR electron densities at conjunction points, binned by magnetic latitude and local time. (a) Mean electron density observed by COSMIC-RO. (b) Mean electron density observed by GRACE-KBR. (c) Mean difference between COSMIC-RO and GRACE-KBR, and (d) number of conjunctions per Mlat-LT bin. In all subplots, the gray background color corresponds to bins with <2 conjunctions.

In the present study, we use the GRACE-KBR data as reference. Our results are in line with those from previous studies, for example, from Habarulema and Carelse (2016). The authors have compared the COSMIC densities to the ionosonde observations during disturbed geomagnetic conditions and concluded that the mean deviation was on the order of 2%–3%, which matches our comparisons in the present study. Since electron densities obtained from COSMIC ROs agree well with GRACE, and they are the only technique that allows evaluating conjunctions on the global scale as well as the biggest data source for empirical modeling collected to date, the other data sources will be compared to COSMIC in the following sections.

4.2. Comparison of CHAMP-PLP and COSMIC-RO Electron Densities

Figure 5 demonstrates a comparison between CHAMP planar Langmuir probe and COSMIC RO electron densities. As before, the scatter plot for all conjunctions is given in Figure 5a, and the normalized occurrence histogram is shown in Figure 5b. We find more than 10,100 conjunctions during geomagnetically quiet times (Kp < 3) across all latitudes and longitudes. The collocations corresponding to low values in CHAMP-PLP data ($N_e < 2 \cdot 10^4$el./cm^3) were removed, to exclude the potential negative bias of CHAMP-PLP at very low densities (see, e.g., McNamara et al., 2007; Pedatella et al., 2015).

From Figure 5a, it can be seen that in general, the scatter points follow a linear trend, although the fitted trend is different from the one-to-one line. The same feature can be observed for the trend fitted to the probability distribution maxima. CHAMP-PLP densities are lower than those observed by COSMIC, with a mean bias of −17,754 el./cm^3, which corresponds to ∼– 10% relative difference. The median bias exhibits roughly similar values of −14,054 el./cm^3, and −12%, respectively (see also Table 2). The Spearman correlation

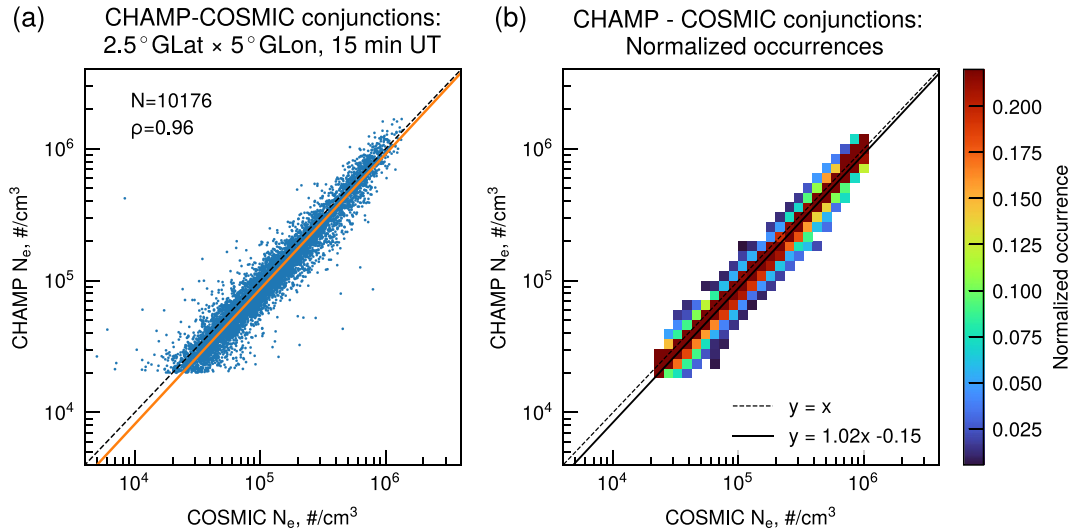

Figure 5. Comparison of CHAMP-PLP and COSMIC-RO densities. Notations are identical to those in Figure 3.

between CHAMP and COSMIC electron densities is high (0.96), indicating that while there is a leveling difference, the behavior of the two data sets is sufficiently similar.

Our results agree well with previous findings. McNamara et al. (2007) compared the CHAMP-PLP plasma frequencies to ionosonde measurements when CHAMP's altitude was below the F2-layer peak. It was found that the CHAMP plasma frequencies were lower than those by the ionosonde, with the majority of the scatter points being higher than the one-to-one line and a bias of around 5%. It should be noted that the bias value of 5% in plasma frequency corresponds to ∼10% difference in electron densities, which matches the bias observed in the present study. Ionosondes provide highly accurate observations of ionospheric densities, and the difference of CHAMP-PLP data with respect to ionosondes justifies the leveling correction presented here.

Pedatella et al. (2015) performed a comparison between the COSMIC and CHAMP electron densities, based on data from 2007 to 2009, although no inter-calibration factors were introduced. In the present study, we use the data from the start of the COSMIC mission in late 2006 until the end of CHAMP operation in 2010. Pedatella et al. (2015) reported that CHAMP electron densities were lower by 14.9%, and the correlation between the two data sets was 0.93, which fits well with our findings. In the present study, our aim is to cross-calibrate data from several missions to further utilize the combined data set for empirical modeling. Therefore, we introduce a linear trend in double-logarithmic scale, and adjust CHAMP-PLP and COSMIC-RO densities using Equation 1 (the coefficients are given in Table 3). Table 4 gives the values of mean and normalized mean bias before and after adjustment. The introduced trend equation helps to eliminate the differences between the data sets, and the relative difference of the adjusted CHAMP-PLP data compared to COSMIC is −3%.

Table 3
Calibration Coefficients Used to Adjust the Data Sets to the Same Reference Frame (GRACE-KBR) Using Equation 1

Data set	*c*	*d*
COSMIC/RO	1	0
CHAMP/PLP	0.980	0.147
CNOFS/CINDI	0.968	0.214
Swarm-A/LP	1.087	−0.380
Swarm-B/LP	1.042	−0.167
Swarm-C/LP	1.087	−0.370

4.3. Comparison of C/NOFS-CINDI and COSMIC-RO Plasma Densities

Figure 6 shows conjunctions between the C/NOFS and COSMIC missions. Figure 6a gives a scatter plot of electron density observed by COSMIC and full ion density measured by the CINDI/RPA instrument aboard C/NOFS. It is apparent that the two data sets are highly consistent with each other, based on the high value of the Spearman correlation (0.97) and a relatively low bias (∼6%). In general, C/NOFS values of electron density are lower than COSMIC observations. Figure 6b shows that, within the range of measurements, the trend fitted to the normalized occurrence histogram generally lies lower than the one-to-one line.

Table 4
Metrics Evaluated Before and After the Adjustment

Comparison	Median bias before correction, el./cm^{-3}	Median bias before correction,%	Median bias after correction, el./cm^{-3}	Median bias after correction,%
CHAMP/PLP - COSMIC/RO	−14,055	−12	−3,538	−3
CNOFS/CINDI - COSMIC/RO	−5,458	−7	45	0
Swarm A/LP - COSMIC/RO	−11,915	−11	−1,192	−1
Swarm B/LP - COSMIC/RO	−4,046	−5	1,371	2
Swarm C/LP - COSMIC/RO	−14,142	−13	−3,236	−3

Our results are consistent with previous findings. Lai et al. (2013) compared C/NOFS-RPA densities to COSMIC-RO observations during 2 consecutive days and reported substantial agreement between them, with a correlation of 0.83 and a slope of the regression line close to 1. While the primary objective of that study was to establish the tentative agreement between the two missions to use both data sets for the analysis of the ionospheric storm that occurred in March 2013, the study showed that the two data sets can be used together in a variety of applications. Pedatella et al. (2015) compared C/NOFS and COSMIC-inferred densities using larger scale statistics for measurements from 2009 to 2013. The two missions were found to be in good agreement, with a correlation of 95% and a relative bias of ∼5.6%. In the present study, we employ a longer data set, comprising collocations between the two missions from 2009 up to the end of C/NOFS operation in 2015, while also using stronger conjunction criteria to decrease the influence of ionospheric gradients. Our results match those of Pedatella et al. (2015). The C/NOFS mission provides a valuable data set of plasma density observations in the topside ionosphere, covering altitudes from 450 to ∼800 km, and can be used together with RO data for empirical topside modeling. Furthermore, several recently launched constellations, for instance, the Ionospheric Connections Explorer (ICON) mission, are equipped with RPAs. The cross-calibration procedure presented here can be employed in future cross-calibration studies and can be used for combined ionospheric monitoring by ICON and the active RO missions, for example, CSES, Spire, and the follow-up constellation COSMIC-2.

4.4. Comparison of Swarm-LP and COSMIC-RO Plasma Densities

Figure 7 shows a comparison between COSMIC electron densities and Swarm ion densities. In the present study, we use observations from 2013 to 2020 and find >3,800 conjunctions during quiet geomagnetic conditions (Kp < 3) for each of the three satellites, distributed across all latitudes and longitudes. Figure 7a shows a scatter plot of electron density measurements from Swarm-A versus COSMIC-RO observations, with data points coming from 06 to 18 LT plotted in orange, and conjunctions occurring at nighttime (18–06 h LT) plotted in blue. Figure 7b shows the normalized occurrences for conjunctions occurring at all MLats during daytime and at |MLat| > 45° during nighttime (explained below and in the Supporting Information S1), with the solid black line representing the linear fit to the probability distribution maxima. In Figure 7a one can observe a somewhat larger scatter on the night side, with a number of points located above the one-to-one line and an overall larger bias than in previous comparisons with GRACE, CHAMP, and C/NOFS. The correlation between Swarm-A and COSMIC densities is high, equal to 0.93, while the percentage bias is on the order of −14%. Figures 7c and 7d demonstrates a similar comparison for Swarm-C. In case of Swarm-C, a roughly similar number of conjunctions was identified, and the bias with respect to COSMIC is −15%. Figures 7e and 7f show the comparison between Swarm-B and COSMIC densities. It is of note that Swarm-B follows an orbit higher by approximately 50 km than those of Swarm-A and -C satellites, and is approximately at 510 km altitude. The correlation between the Swarm-B and COSMIC plasma densities is lower than that for A and C satellites and equals 0.86. Conversely, the mean value of bias is lower for Swarm-B compared to A and C spacecraft and equals −8%. However, it should be noted that the difference between COSMIC and Swarm-B depends on local time, with an underestimation by Swarm-B on the dayside and a stronger overestimation on the nightside. The standard deviation for Swarm-B is ∼55%, which is higher than for spacecraft A and C for which it is approximately 45%.

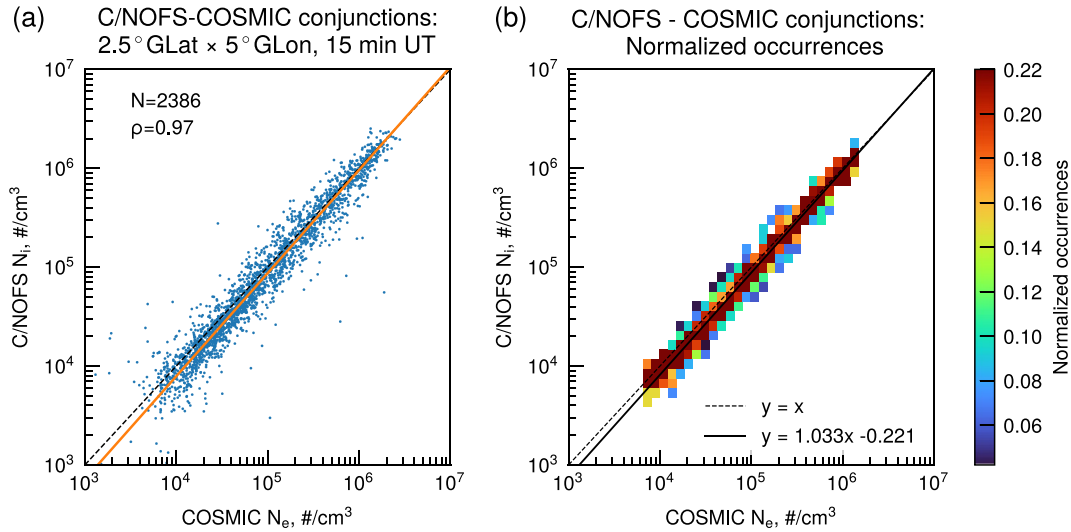

Figure 6. Comparison of CNOFS/CINDI and COSMIC-RO densities. Notations are the same as in Figure 3.

In previous studies, Swarm ion densities were compared to the ISR and ionosonde observations during December 2013 to June 2016 period, and the offset between Swarm and ground-based measured densities was noticeable both for ionosondes and ISRs (Lomidze et al., 2018). The corrections were introduced based on conjunctions between each of the Swarm satellites and the ISRs. The adjusted Swarm ion densities were compared to COSMIC RO observations at ~2,000 collocations. In the present study, we employ a longer data set for the comparison (from 2013 to 2019), which yields approximately two times more conjunctions with COSMIC. The correction factors, introduced by Lomidze et al. (2018), were uniform with respect to local time and latitude, as Swarm satellites were found to underestimate densities by a factor of ~1.1 at conjunctions with the ISRs. Figures 7a, 7c, and 7e indicate that on the night side, all three Swarm satellites may overestimate densities, and this effect is most prominent for Swarm-B. To investigate this LT-dependent difference in more detail, we analyze the distribution of the mean and relative (%) bias between Swarm and COSMIC as a function of magnetic latitude and local time.

Figure 8 demonstrates the difference between Swarm and COSMIC plasma density data at conjunctions, binned by 5°MLat–1h LT. In the comparison with GRACE-KBR (Figure 4), COSMIC was found to slightly underestimate the crests of the equatorial ionization anomaly as a result of the Abel inversion. In Figure 8, the opposite effect is observed. Swarm densities are lower than COSMIC around the geomagnetic equator at daytime (6–18 LT). At middle latitudes, Swarm measurements are also lower than COSMIC observations. Furthermore, on the nightside (18–06 LT) all three Swarm satellites exhibit higher densities than COSMIC. Figures 8a and 8d indicate that these patterns are highly consistent for Swarm-A and Swarm-C satellites, due to their similar orbital height (460 km) and small spatial separation of 1.4° GLon. The EIA underestimation on the dayside is of the order of $1 - 2 \cdot 10^5$ el./cm^3, which corresponds to approximately 10 – 30% relative bias. On the nightside, the overestimation is in the order of $0.3 \cdot 10^5$ el./cm^3 (10%–20%).

The overestimation of Swarm-B at nightside (Figure 8g) is higher than in case of A and C satellites (~$0.5 \cdot 10^5$ el./cm^3 compared to ~$0.3 \cdot 10^5$ el./cm^3). While at middle and equatorial latitudes Swarm-A densities were larger than COSMIC observations by 10%–20%, the overestimation by Swarm-B is often >40%. As noted above, Swarm A and C follow a roughly similar orbit, and their elevation after the commissioning phase is ~460 km. Swarm-B is at an altitude of ~510km. One of the potential reasons for the larger electron density overestimation by Swarm-B compared to A and C satellites is related to lower oxygen-hydrogen transition heights at low and mid-latitudes during nighttime compared to daytime (~500km vs. >850 km; e.g., Aponte et al., 2013; Heelis et al., 2009). The Swarm LPs are assumed to measure O^+ ions exclusively and therefore at heights below ~500 km where this assumptions holds the difference between Swarm A and C with respect to COSMIC is lower than at 510 km where the H^+ and He^+ play an important role in the ion composition and would lead to larger overestimation at nightside by Swarm-B. Another effect that can contribute to this

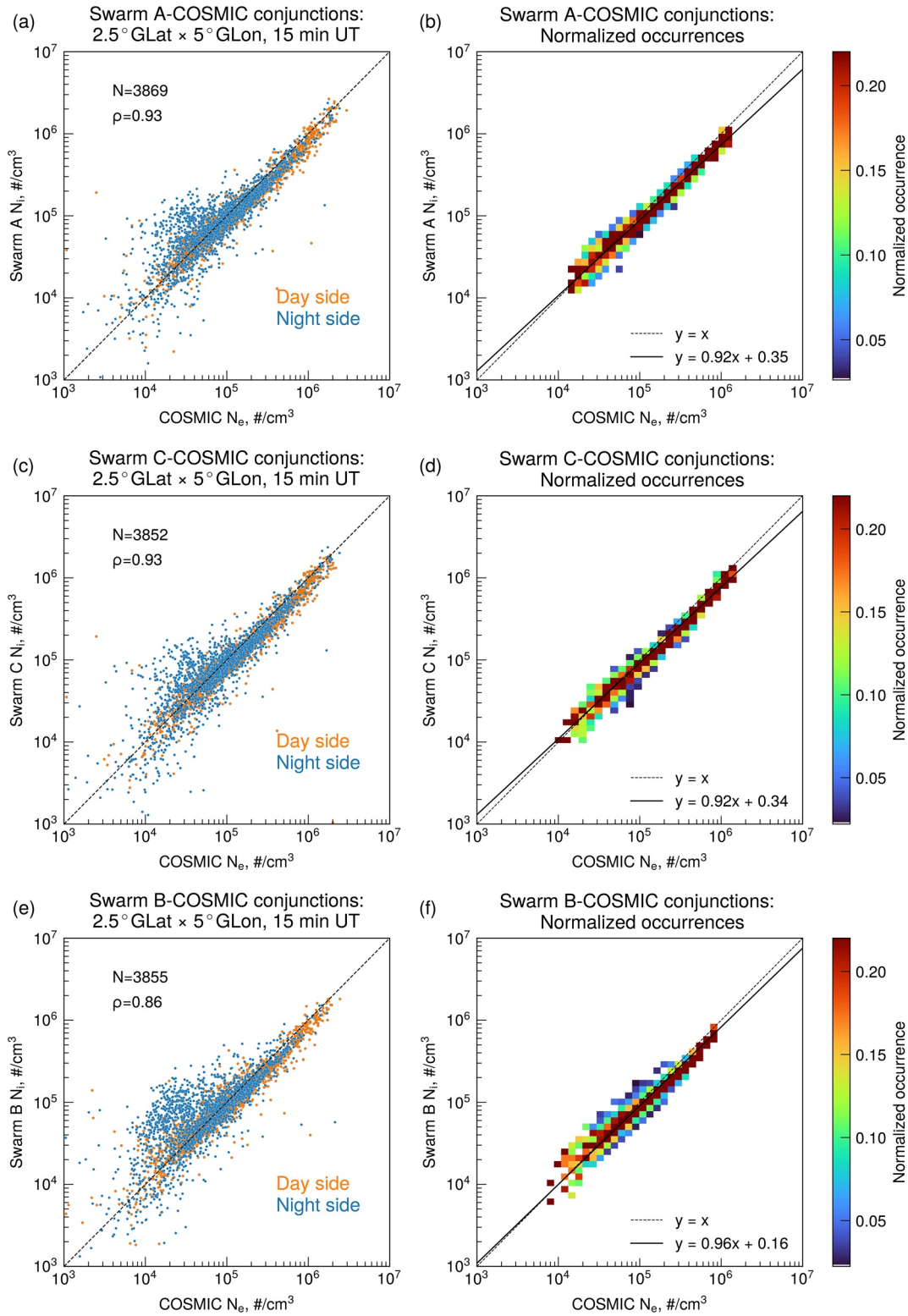

Figure 7. Comparison of Swarm-A ion densities and COSMIC-RO electron densities. (a, c, e) Scatter plot of Swarm A, C, and B versus COSMIC-RO densities. The conjunctions at nightside (18–06 LT) are shown in blue, and those at dayside (06–18 LT) are plotted in orange. The dashed line represents one-to-one ratio between the data sets. (b, d, f) Normalized occurrence plot of Swarm A, C, and B versus COSMIC-RO densities based on conjunctions occurring at all MLats at dayside and at | MLat |> 45° at nightside. The trend fitting procedure is the same as in Figure 3.

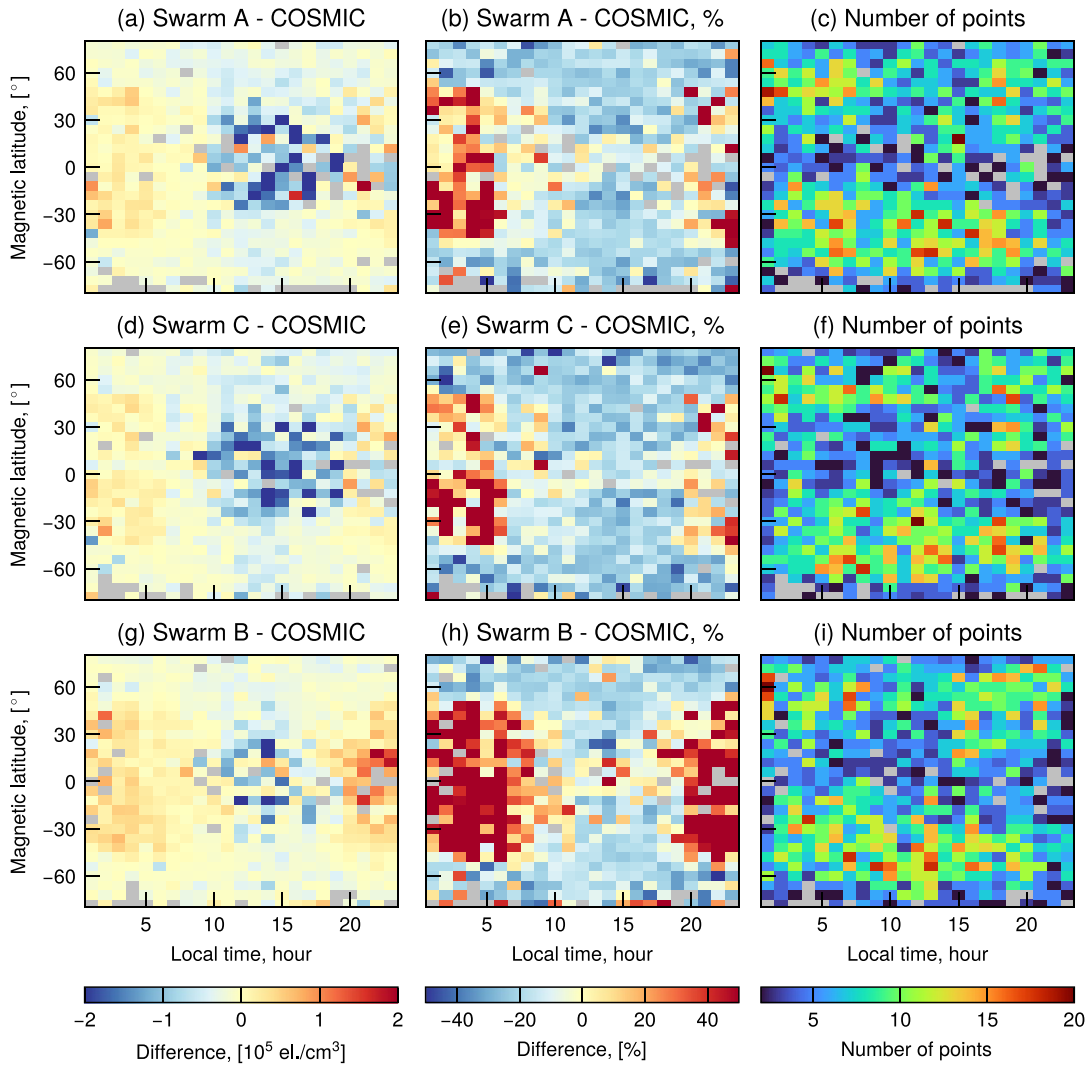

Figure 8. Comparison between Swarm-LP and COSMIC-RO plasma densities, binned by 5° MLat-1h LT. Mean bias (a, d, g), mean percentage bias (b, e, h), and number of conjunctions in bin (c, f, i) for Swarm A, C, and B satellites, respectively.

overestimation is the influence of the spacecraft potential, which depends on the illumination of the solar cells and could lead to density overestimation at night side.

In Table 4, we demonstrate the median bias before and after applying the proposed calibration coefficients, evaluated on all conjunctions. It can be seen that for all three Swarm satellites the proposed corrections reduce bias to the 1%–3% range. Therefore, it can be concluded that while the linear correction factors for Swarm match the probability distribution maxima and eliminate most of the bias, a more detailed analysis on the separation between oxygen and hydrogen/helium ions within Swarm's electric field instrument (EFI) and effects of the spacecraft potential needs to be performed in future studies.

5. Summary and Conclusions

Over the last 20 years, the Earth's ionosphere has become a data-rich environment, as the total number of plasma density measurements is approaching several billion points. This wealth of observations, provided by direct in situ (LP, RPA) and remote sensing (RO) techniques, presents new opportunities for the large-scale empirical modeling. Yet, in the topside ionosphere, the altitude distribution of data remains far from uniform. To compensate for the uneven coverage it is essential to utilize all of the available observations in

modeling, and therefore these data sources need to be adjusted to the same reference frame. Since the measurement and calibration techniques are specific to each instrument, a reliable long-term plasma density data set is needed to perform the intercalibration.

In this study, we use the GRACE-KBR electron density measurements as a reference data set. The KBR data have been thoroughly validated by the ISR measurements and represent a practically calibration-free data set, providing electron densities at 400–500 km altitude over ~1.5 solar cycles in 2002–2017. As a reference data set for the intercalibration, satellite electron density observations by GRACE-KBR have notable advantages over the ground-based ISR data, such as, for instance, the global coverage in the topside ionosphere.

The comparison of the RO data from COSMIC mission to the reference KBR data set shows an excellent agreement between them. Although COSMIC slightly underestimates the EIA crests, the two missions are highly consistent with a mean percentage difference of ~2%. This indicates that first, the two missions can be used in combination for empirical modeling, and second, other data sources can be compared to COSMIC-1. We find that CHAMP-PLP densities are lower than those provided by COSMIC by ~11%, and introduce simple inter-calibration factors between them. C/NOFS-CINDI ion densities are generally in good agreement with COSMIC, although the trend between them is different from the one-to-one line. Swarm ion densities have been compared to COSMIC at a large number of conjunctions (>3800 collocations for each of the satellites). It was found that while the corrections from previous studies, as well as the calibration factors introduced here based on the probability distribution functions, remove most of the bias, the difference between Swarm and COSMIC has local-time signatures which are strongest for Swarm-B. Amongst the potential reasons for such an effect, there are LT-variations in upper transition height, or influence of the spacecraft potential, and more detailed investigations can be performed in future studies.

The calibration factors introduced in this study (Table 3) can have wide applications in ionospheric research. They eliminate the systematic leveling differences between the most prominent and widely used ionospheric data sets. Hence, these data can be used jointly to set up new highly accurate models of electron density, for example, those based on machine learning. Furthermore, they allow a more precise in-orbit model validation for the existing models. Moreover, the ongoing follow-up mission GRACE-FO allows density retrieval by the same technique as the original GRACE mission, and can be used as a reference for calibrating the recently launched or planned ionospheric constellations. Several active missions carry instruments that operate on the same principles as the ones analyzed in the present study. Therefore, an approach developed in this study could be extended to other new in situ data sets, for instance, the NASA's ICON-RPA data, allowing for a complex ionospheric monitoring by the GRACE-FO, ICON, and the active RO missions, such as CSES, Spire, and COSMIC-2.

Data Availability Statement

The GRACE electron density data have been provided in the framework of the Topside Ionosphere Radio Observations from multiple LEO-missions (TIRO) project funded by ESA via the Swarm DISC, Sub-Contract No. SW-CO-DTU-GS-126, and are accessible at (Xiong et al., 2021). The Level 2 CHAMP PLP data are publicly available at Rother and Michaelis (2019) and through the Information System and Data Centre (ISDC) of GFZ Potsdam (https://isdc.gfz-potsdam.de/champ-isdc/). Swarm LP data were obtained from ESA (https://earth.esa.int/web/guest/swarm/data-access). C/NOFS data were obtained through NASA's Space Physics Data Facility (SPDF, spdf.gsfc.nasa.gov). The F10.7 index was downloaded from the OMNIWeb database (omniweb.gsfc.nasa.gov). COSMIC data can be downloaded via UCAR (https://cdaac-www.cosmic.ucar.edu/).

Acknowledgments
This study is supported by the Helmholtz Pilot Projects Information & Data Science II, MAchine learning based Plasma density model project (MAP) – ZT-I-0022. The COSMIC data set is based upon work supported by the National Center for Atmospheric Research, which is a major facility sponsored by the U.S. National Science Foundation under Cooperative Agreement 1852977. N. Pedatella acknowledges support from AFOSR grant FA9550-16-1-0050 and US National Science Foundation grant AGS-1522830. Open access funding enabled and organized by Projekt DEAL.

References

Aponte, N., Brum, C. G., Sulzer, M. P., & González, S. A. (2013). Measurements of the O^+ to H^+ transition height and ion temperatures in the lower topside ionosphere over Arecibo for equinox conditions during the 2008–2009 extreme solar minimum. *Journal of Geophysical Research: Space Physics*, *118*(7), 4465–4470. https://doi.org/10.1002/jgra.50416

Arras, C., Jacobi, C., Wickert, J., Heise, S., & Schmidt, T. (2010). Sporadic E signatures revealed from multi-satellite radio occultation measurements. *Advances in Radio Science*, *8*, 225–230. https://doi.org/10.5194/ars-8-225-2010

Astafyeva, E. (2019). Ionospheric detection of natural hazards. *Reviews of Geophysics*, *57*(4), 1265–1288. https://doi.org/10.1029/2019rg000668

Benson, R. F., & Bilitza, D. (2009). New satellite mission with old data: Rescuing a unique data set. *Radio Science*, *44*(01), 1–14. https://doi.org/10.1029/2008rs004036

Bilitza, D. (2018). IRI the International Standard for the Ionosphere. *Advances in Radio Science*, *16*, 1–11. https://doi.org/10.5194/ars-16-1-2018

Bilitza, D., & Xiong, C. (2021). A solar activity correction term for the IRI topside electron density model. *Advances in Space Research*. *68*(5), 2124–2137.

Cherniak, I., & Zakharenkova, I. (2019). Evaluation of the IRI-2016 and NeQuick electron content specification by COSMIC GPS radio occultation, ground-based GPS and Jason-2 joint altimeter/GPS observations. *Advances in Space Research*, *63*(6), 1845–1859. https://doi.org/10.1016/j.asr.2018.10.036

Cherniak, I., Zakharenkova, I., Braun, J., Wu, Q., Pedatella, N., Schreiner, W., et al. (2021). Accuracy assessment of the quiet-time ionospheric F2 peak parameters as derived from COSMIC-2 multi-GNSS radio occultation measurements. *Journal of Space Weather and Space Climate*, *11*, 18. https://doi.org/10.1051/swsc/2020080

Cherniak, I. V., & Zakharenkova, I. (2014). Validation of FORMOSAT-3/COSMIC radio occultation electron density profiles by incoherent scatter radar data. *Advances in Space Research*, *53*(9), 1304–1312. https://doi.org/10.1016/j.asr.2014.02.010

Cherniak, I. V., Zakharenkova, I., Krankowski, A., & Shagimuratov, I. (2012). Plasmaspheric electron content derived from GPS TEC and FORMOSAT-3/COSMIC measurements: Solar minimum condition. *Advances in Space Research*, *50*(4), 427–440. https://doi.org/10.1016/j.asr.2012.04.002

Chuo, Y.-J., Lee, C.-C., Chen, W.-S., & Reinisch, B. W. (2011). Comparison between bottomside ionospheric profile parameters retrieved from FORMOSAT3 measurements and ground-based observations collected at Jicamarca. *Journal of Atmospheric and Solar-Terrestrial Physics*, *73*(13), 1665–1673. https://doi.org/10.1016/j.jastp.2011.02.021

Coley, W., Heelis, R., Hairston, M., Earle, G., Perdue, M., Power, R., et al. (2010). Ion temperature and density relationships measured by cindi from the C/NOFS spacecraft during solar minimum. *Journal of Geophysical Research*, *115*(A2). https://doi.org/10.1029/2009ja014665

Costa, E., Roddy, P., & Ballenthin, J. (2014). Statistical analysis of C/NOFS planar Langmuir probe data. *Annales Geophysicae*, *32*, 773–791. https://doi.org/10.5194/angeo-32-773-2014

de La Beaujardière, O., & the C/NOFS Science Definition Team. (2004). C/NOFS: A mission to forecast scintillations. *Journal of Atmospheric and Solar-Terrestrial Physics*, *66*(17), 1573–1591. https://doi.org/10.1016/j.jastp.2004.07.030

Forsythe, V. V., Duly, T., Hampton, D., & Nguyen, V. (2020). Validation of ionospheric electron density measurements derived from Spire CubeSat constellation. *Radio Science*, *55*(1), e2019RS006953. https://doi.org/10.1029/2019rs006953

Friis-Christensen, E., Lühr, H., & Hulot, G. (2006). Swarm: A constellation to study the Earth's magnetic field. *Earth, Planets and Space*, *58*(4), 351–358. https://doi.org/10.1186/bf03351933

Goss, A., Schmidt, M., Erdogan, E., Görres, B., & Seitz, F. (2019). High-resolution vertical total electron content maps based on multi-scale B-spline representations. *Annales Geophysicae*, *37*(4). https://doi.org/10.5194/angeo-37-699-2019

Habarulema, J. B., & Carelse, S. A. (2016). Long-term analysis between radio occultation and ionosonde peak electron density and height during geomagnetic storms. *Geophysical Research Letters*, *43*(9), 4106–4111. https://doi.org/10.1002/2016gl068944

Hajj, G., Kursinski, E., Bertiger, W., Leroy, S., Meehan, T., Romans, L., & Schofield, J. (1996). Initial results of GPS-LEO occultation measurements of Earth's atmosphere obtained with the GPS-MET experiment. In: *GPS trends in precise terrestrial, airborne, and spaceborne applications* (pp. 144–153). Springer. https://doi.org/10.1007/978-3-642-80133-4_23

Hargreaves, J. K. (1992). *The solar-terrestrial environment: An introduction to geospace-the science of the terrestrial upper atmosphere, ionosphere, and magnetosphere*. Cambridge University Press.

Heelis, R., Coley, W., Burrell, A., Hairston, M., Earle, G., Perdue, M., et al. (2009). Behavior of the O^+/H^+ transition height during the extreme solar minimum of 2008. *Geophysical Research Letters*, *36*(18). https://doi.org/10.1029/2009gl038652

Hernández-Pajares, M., Juan, J. M., Sanz, J., Aragón-Àngel, À., García-Rigo, A., Salazar, D., & Escudero, M. (2011). The ionosphere: Effects, GPS modeling and the benefits for space geodetic techniques. *Journal of Geodesy*, *85*(12), 887–907. https://doi.org/10.1007/s00190-011-0508-5

Hobiger, T., & Jakowski, N. (2017). Atmospheric signal propagation. In: *Springer handbook of global navigation satellite systems* (pp. 165–193). Springer. https://doi.org/10.1007/978-3-319-42928-1_6

Jakowski, N., Wehrenpfennig, A., Heise, S., Reigber, C., Lühr, H., Grunwaldt, L., & Meehan, T. (2002). GPS radio occultation measurements of the ionosphere from CHAMP: Early results. *Geophysical Research Letters*, *29*(10), 95-1–95-4. https://doi.org/10.1029/2001gl014364

Kashcheyev, A., & Nava, B. (2019). Validation of NeQuick 2 model topside ionosphere and plasmasphere electron content using COSMIC POD TEC. *Journal of Geophysical Research: Space Physics*, *124*(11), 9525–9536. https://doi.org/10.1029/2019ja026971

Kelley, M., Wong, V., Aponte, N., Coker, C., Mannucci, A., & Komjathy, A. (2009). Comparison of COSMIC occultation-based electron density profiles and TIP observations with Arecibo incoherent scatter radar data. *Radio Science*, *44*(4). https://doi.org/10.1029/2008rs004087

Kivelson, M., & Russell, C. (1995). *Introduction to space physics*. Cambridge University Press.

Klimenko, M., Klimenko, V., Zakharenkova, I., & Cherniak, I. V. (2015). The global morphology of the plasmaspheric electron content during Northern winter 2009 based on GPS/COSMIC observation and GSM TIP model results. *Advances in Space Research*, *55*(8), 2077–2085. https://doi.org/10.1016/j.asr.2014.06.027

Knudsen, D., Burchill, J., Buchert, S., Eriksson, A., Gill, R., Wahlund, J.-E., et al. (2017). Thermal ion imagers and Langmuir probes in the Swarm electric field instruments. *Journal of Geophysical Research: Space Physics*, *122*(2), 2655–2673. https://doi.org/10.1002/2016ja022571

Lai, P.-C., Burke, W. J., & Gentile, L. (2013). Topside electron density profiles observed at low latitudes by COSMIC and compared with in situ ion densities measured by C/NOFS. *Journal of Geophysical Research: Space Physics*, *118*(5), 2670–2680. https://doi.org/10.1002/jgra.50287

Lee, H.-B., Jee, G., Kim, Y. H., & Shim, J. (2013). Characteristics of global plasmaspheric TEC in comparison with the ionosphere simultaneously observed by Jason-1 satellite. *Journal of Geophysical Research: Space Physics*, *118*(2), 935–946. https://doi.org/10.1002/jgra.50130

Lei, J., Syndergaard, S., Burns, A. G., Solomon, S. C., Wang, W., Zeng, Z., et al. (2007). Comparison of COSMIC ionospheric measurements with ground-based observations and model predictions: Preliminary results. *Journal of Geophysical Research*, *112*(A7). https://doi.org/10.1029/2006ja012240

Liu, J., Lin, C., Lin, C., Tsai, H., Solomon, S., Sun, Y., et al. (2010). Artificial plasma cave in the low-latitude ionosphere results from the radio occultation inversion of the FORMOSAT-3/COSMIC. *Journal of Geophysical Research*, *115*(A7). https://doi.org/10.1029/2009ja015079

Lomidze, L., Knudsen, D. J., Burchill, J., Kouznetsov, A., & Buchert, S. C. (2018). Calibration and validation of Swarm plasma densities and electron temperatures using ground-based radars and satellite radio occultation measurements. *Radio Science*, *53*(1), 15–36. https://doi.org/10.1002/2017rs006415

McNamara, L., Cooke, D., Valladares, C., & Reinisch, B. (2007). Comparison of CHAMP and Digisonde plasma frequencies at Jicamarca, Peru. *Radio Science*, *42*(2), 1–14. https://doi.org/10.1029/2006rs003491

Melbourne, W., Davis, E., Duncan, C., Hajj, G., Hardy, K., Kursinski, E., et al. (1994). The application of spaceborne GPS to atmospheric limb sounding and global change monitoring.

Moosavi, S. M., & Ghassabian, S. (2018). Linearity of calibration curves for analytical methods: A review of criteria for assessment of method reliability. In: *Calibration and validation of analytical methods – A sampling of current approaches* (pp. 109–127). IntechOpen Ltd.

Nava, B., Coisson, P., & Radicella, S. (2008). A new version of the NeQuick ionosphere electron density model. *Journal of Atmospheric and Solar-Terrestrial Physics*, *70*(15), 1856–1862. https://doi.org/10.1016/j.jastp.2008.01.015

Pedatella, N., Yue, X., & Schreiner, W. (2015). Comparison between GPS radio occultation electron densities and in situ satellite observations. *Radio Science*, *50*(6), 518–525. https://doi.org/10.1002/2015rs005677

Petit, G., & Luzum, B. (2010). *IERS conventions*. Retrieved from www.iers.org

Prol, F. S., Themens, D. R., Hernández-Pajares, M., de Oliveira Camargo, P., & Muella, M. T. D. A. H. (2019). Linear Vary-Chap topside electron density model with topside sounder and radio-occultation data. *Surveys in Geophysics*, *40*(2), 277–293. https://doi.org/10.1007/s10712-019-09521-3

Reigber, C., Lühr, H., Schwintzer, P., & Wickert, J. (2004). Earth observation with CHAMP. Results from three years.

Rother, M., & Michaelis, I. (2019). Ch-me-2-plpt-champ electron density and temperature time series in low time resolution (level 2). https://doi.org/10.5880/GFZ.2.3.2019.004

Rother, M., Schlegel, K., Lühr, H., & Cooke, D. (2010). Validation of CHAMP electron temperature measurements by incoherent scatter radar data. *Radio Science*, *45*(6), 1–10. https://doi.org/10.1029/2010rs004445

Schreiner, W. S., Rocken, C., Sokolovskiy, S., Syndergaard, S., & Hunt, D. (2007). Estimates of the precision of GPS radio occultations from the COSMIC/FORMOSAT-3 mission. *Geophysical Research Letters*, *34*(4). https://doi.org/10.1029/2006gl027557

Schreiner, W. S., Weiss, J., Anthes, R. A., Braun, J., Chu, V., Fong, J., et al. (2020). COSMIC-2 radio occultation constellation: First Results. *Geophysical Research Letters*, *47*(4), e2019GL086841. https://doi.org/10.1029/2019gl086841

Shim, J., Scherliess, L., Schunk, R., & Thompson, D. (2008). Spatial correlations of day-to-day ionospheric total electron content variability obtained from ground-based GPS. *Journal of Geophysical Research*, *113*(A9). https://doi.org/10.1029/2007ja012635

Smirnov, A. G., Berrendorf, M., Shprits, Y., Kronberg, E. A., Allison, H. J., Aseev, N. A., et al. (2020). Medium energy electron flux in Earth's outer radiation belt (MERLIN): A machine learning model. *Space Weather*, *18*(11), e2020SW002532. https://doi.org/10.1029/2020sw002532

Wang, X., Cheng, W., Zhou, Z., Xu, S., Yang, D., & Cui, J. (2019). Comparison of CSES ionospheric RO data with COSMIC measurements. *Annales Geophysicae*, *37*, 1025–1038. https://doi.org/10.5194/angeo-37-1025-2019

Xiong, C., Lühr, H., Ma, S., & Schlegel, K. (2015). Validation of GRACE electron densities by incoherent scatter radar data and estimation of plasma scale height in the topside ionosphere. *Advances in Space Research*, *55*(8), 2048–2057. https://doi.org/10.1016/j.asr.2014.07.022

Xiong, C., Lühr, H., & Stolle, C. (2021). GRACE electron density derived from the K-band ranging system (KBR).

Xiong, C., Park, J., Lühr, H., Stolle, C., & Ma, S. (2010). Comparing plasma bubble occurrence rates at CHAMP and GRACE altitudes during high and low solar activity. *Annales Geophysicae*, *28*, 1647–1658. https://doi.org/10.5194/angeo-28-1647-2010

Yizengaw, E., Moldwin, M., Galvan, D., Iijima, B., Komjathy, A., & Mannucci, A. (2008). Global plasmaspheric TEC and its relative contribution to GPS TEC. *Journal of Atmospheric and Solar-Terrestrial Physics*, *70*(11–12), 1541–1548. https://doi.org/10.1016/j.jastp.2008.04.022

Yue, X., Schreiner, W. S., Lei, J., Sokolovskiy, S. V., Rocken, C., Hunt, D. C., & Kuo, Y.-H. (2010). Error analysis of Abel retrieved electron density profiles from radio occultation measurements. *Annales Geophysicae*, *28*, 217–222. https://doi.org/10.5194/angeo-28-217-2010